CHEMISTRY
A EUROPEAN JOURNAL

# Supporting Information



## Probing the Dynamics of $CO_2$ and $CH_4$ within the Porous Zirconium Terephthalate UiO-66(Zr): A Synergic Combination of Neutron Scattering Measurements and Molecular Simulations

**Qingyuan Yang,[a, d] Hervé Jobic,*[b] Fabrice Salles,[a] Daniil Kolokolov,[b, e] Vincent Guillerm,[c] Christian Serre,[c] and Guillaume Maurin*[a]**

chem_201003596_sm_miscellaneous_information.pdf

## 1. Sample preparation

UiO-66(Zr) was prepared from a large scale mixture of zirconium tetrachloride $ZrCl_4$, terephthalic acid $HO_2CC_6H_4$-$CO_2H$, hydrochloric acid and dimethylformamide in the 25 mmol : 50 mmol : 50 mmol : 150 mL ratio. The slurry was then introduced in a 750 mL Teflon liner and further introduced in a metallic PAAR bomb. The system was heated overnight (16h) at 220 °C. The resulting white product was filtered off, washed with DMF to remove the excess of unreacted terephthalic acid, then washed again with acetone and dried at room temperature. The sample was finally calcined at 250°C under vacuum (5 mbar) to remove the DMF from the framework. X-Ray powder diffractogram (Brüker D5000, $\lambda_{Cu}\approx1.5406$ Å) of the sample is in a very good agreement with the one calculated from the published structure.[1] Nitrogen sorption measurments (BelSorp Max apparatus) gave a BET surface area of 1067(3) $m^2/g$.

## 2. Quasi-elastic neutron scattering measurements

The QENS measurements were carried out using the time-of-flight spectrometer IN6, at the Institut Laue-Langevin, Grenoble, France. Since the scattering from $CO_2$ is weak, a deuterated analogue of UiO-66(Zr) was prepared to reduce the scattering from the MOF framework. On IN6, the incident neutron energy was set to 3.12 meV, corresponding to a wavelength of 5.12 Å. After scattering by the sample, the neutrons are analyzed as a function of flight time and angle. The wave-vector transfer *Q* varies with the scattering angle and ranged from 0.25 to 1.2 $Å^{-1}$. Different spectra were grouped to obtain satisfactory counting statistics. Detectors corresponding to the Bragg peaks of UiO-66(Zr) were avoided as much as possible, but the dehydroxylation of this MOF lowers the space group so that elastic intensity was found at low *Q*. Time-of-flight spectra were converted to energy spectra. The elastic energy resolution was

measured with a vanadium standard, it could be fitted by a Gaussian function, with a half-width at half-maximum varying from 40 μeV at small $Q$ to 50 μeV at large $Q$.

The UiO-66(Zr) sample was activated by pumping at 473 K, the final pressure being better than $10^{-3}$ Pa after cooling. The degassed MOF was transferred inside a glovebox into a slab-shaped aluminium container, which was connected to a gas inlet system, allowing *in situ* adsorption. After recording the scattering of the empty material, different loadings of $CO_2$ (6.9, 21.4, 35.7, 38 $CO_2$/u.c., respectively) were investigated at 230 K, the adsorbed amounts being determined by volumetry. After these runs, $CO_2$ was evacuated by pumping the cell at 370 K. After desorption, it was checked that the signal of the degassed MOF was identical to the original UiO-66(Zr) solid. $CH_4$ was then measured at various concentrations (4.4, 8.4, 10.5, 16.5 $CH_4$/u.c., respectively) at 230 K. One can follow the mobility of individual $CH_4$ molecules since the scattering is dominated by the large incoherent cross section of hydrogen, and thus its self-diffusion coefficients can be extracted. $CO_2$ is a totally coherent scatterer so that the collective mobility of $CO_2$ in UiO-66 can be extracted from the QENS data. It is the transport diffusivity ($D_t$) of $CO_2$ which is obtained, since one probes the time evolution of the density fluctuations which occur at equilibrium.[2]

To illustrate differently the fact that the broadening of the elastic peak increases up to the third loading, and then decreases, the half-width at half-maximum (HWHM) of spectra obtained at two different values of the wave-vector transfer $Q$, are shown in Figure S1. In this representation, it also appears that the maximum is observed for 10.5 molecules/u.c., corresponding to a maximum in diffusivity.

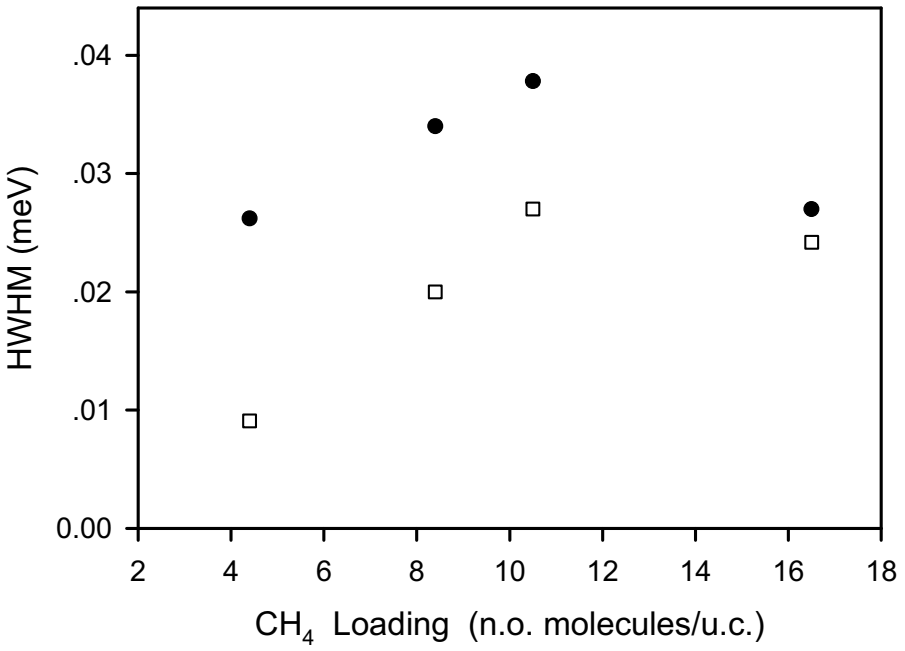


***Figure S1.*** Half-width at half-maximum of QENS spectra obtained at two different *Q* values: (□) 0.25, (●) 0.45 $Å^{-1}$, as a function of methane loading.

## 3. Partial charges for the framework atoms

The Mulliken partial charges carried by all the atoms of the dehydroxylated UiO-66(Zr) were taken from our previous density functional theory (DFT) calculation.[3] In this calculation, the $Dmol^3$ code implemented in Accelrys Material Studio was employed to perform such calculations, that are based on the PW91 GGA functional combined with the double numerical basis set containing polarisation function (DNP). The resulting charges are reported in Table S1, the location of each atom type on the hybrid framework being described in Figure S2.

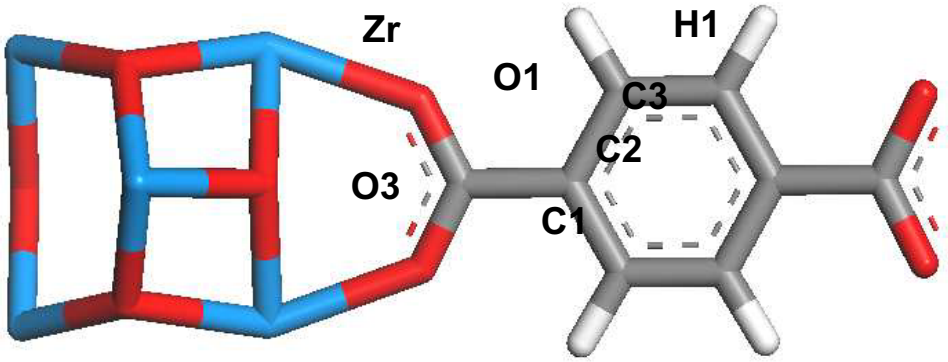


***Figure S2.*** Labels of the atoms for the inorganic and organic parts of the dehydroxylated UiO-66(Zr), corresponding to the atomic types given in Table *S1*.

**Table *S1***. Partial charges carried by each atomic type of the dehydroxylated UiO-66(Zr) framework.

| Atomic types | Zr | C1 | C2 | C3 | O1 | O3 | H1 |
|---|---|---|---|---|---|---|---|
| Charges (*e*) | 1.968 | 0.630 | -0.082 | -0.065 | -0.586 | -0.992 | 0.133 |

## 4. Interatomic potentials

In this present work, the forcefields used for the adsorbate species are the same as those adopted in our previous work.[3] That is, a single Lennard-Jones (LJ) interaction site model was used to describe a $CH_4$ molecule with potential parameters taken from the TraPPE forcefield;[4] while $CO_2$ molecule was represented by the conventional rigid linear triatomic model with three charged LJ interaction sites (C–O bond length of 1.149 Å) located on each atom as previously described by Harris and Yung.[5] All the corresponding atomic partial charges and interatomic potential parameters are reported in Table *S2*.

An atomistic representation was used to model the dehydroxylated UiO-66(Zr) material with the crystallographic coordinates taken from the DFT optimized structure in our previous study.[3] The interaction between $CO_2$ and the UiO-66(Zr) surface was described by a combination of site-site LJ and Coulombic potentials,

$$U_{ij}^{non-bonded} = 4\varepsilon_{ij}\left[\left(\frac{\sigma_{ij}}{r_{ij}}\right)^{12} - \left(\frac{\sigma_{ij}}{r_{ij}}\right)^{6}\right] + \frac{q_i q_j}{r_{ij}} \quad (1)$$

while the $CH_4$/UiO-66(Zr) interaction was only treated using a site-site LJ potential. The synthesized sample is of high quality with both pore volume and surface area very similar to the predicted ones. From this point, one can test which generic forcefield does a better job by a direct comparison between simulated and experimental isotherms. With this in mind, we selected the most appropriate forcefields as follows:

(1) **For $CH_4$**: Figure S3a shows the comparison of the simulated adsorption isotherm with the experimental data. Obviously, the simulations based on the DREIDING forcefield[6] for representing the framework are in a very good agreement the experimental data, while those using the UFF[7] forcefield lead to an overestimation of the adsorbed amounts. In addition, when one deals with the adsorption of $CH_4$ or alkanes in MOF materials, one can find in the literature that the description of the framework via the DREIDING forcefield usually leads to a better agreement with the experimental results[8, 9] Thus, based on these conclusions, the DREIDING forcefield was adopted for the framework in order to calculate the cross LJ terms for the $CH_4$-MOF interaction.

(2) **For $CO_2$**: Figure S3b indicates that the overall agreement between the simulated adsorption isotherms and experimental data is better using the UFF forcefield than the DREIDING one. In addition, one can find in the literature that the simulations based on the UFF forcefield for describing the MOF framework lead to a better agreement with the experimental data on the $CO_2$ adsorption in various MOFs.[10-12] Thus, based on these conclusions, the UFF forcefield was adopted for the framework in order to calculate the cross LJ terms for the $CO_2$-MOF interaction.

The corresponding potential parameters for the framework atoms are listed in Table S2. All the LJ cross interaction parameters including adsorbate/adsorbate and adsorbate/MOF were determined by the Lorentz-Berthelot mixing rule.

***Table S2.*** Potential parameters and partial charges for the adsorbates

| **Atomic type** | $\sigma$ **(Å)** | $\varepsilon$ **(kJ/mol)** | ***q*(*e*)** |
|---|---|---|---|
| $CH_4$ | 3.730 | 1.230 | 0.0000 |
| CO2_C | 2.757 | 0.234 | 0.6512 |
| CO2_O | 3.033 | 0.669 | -0.3256 |

***Table S3***. Lennard-Jones (LJ) potential parameters for the framework atoms in the dehydroxylated UiO-66(Zr) framework.

| **Atomic types** | **DREIDING** | | **UFF** | |
|---|---|---|---|---|
| | $\sigma$ **(Å)** | $\varepsilon$ **(kJ/mol)** | $\sigma$ **(Å)** | $\varepsilon$ **(kJ/mol)** |
| Zr | 2.783[a] | 0.2887[a] | 2.783 | 0.2887 |
| C1 | 3.473 | 0.3979 | 3.431 | 0.4393 |
| C2 | 3.473 | 0.3979 | 3.431 | 0.4393 |
| C3 | 3.473 | 0.3979 | 3.431 | 0.4393 |
| O1 | 3.033 | 0.4004 | 3.118 | 0.2510 |
| O3 | 3.033 | 0.4004 | 3.118 | 0.2510 |
| H1 | 2.846 | 0.0636 | 2.571 | 0.1841 |

[a] taken from UFF.

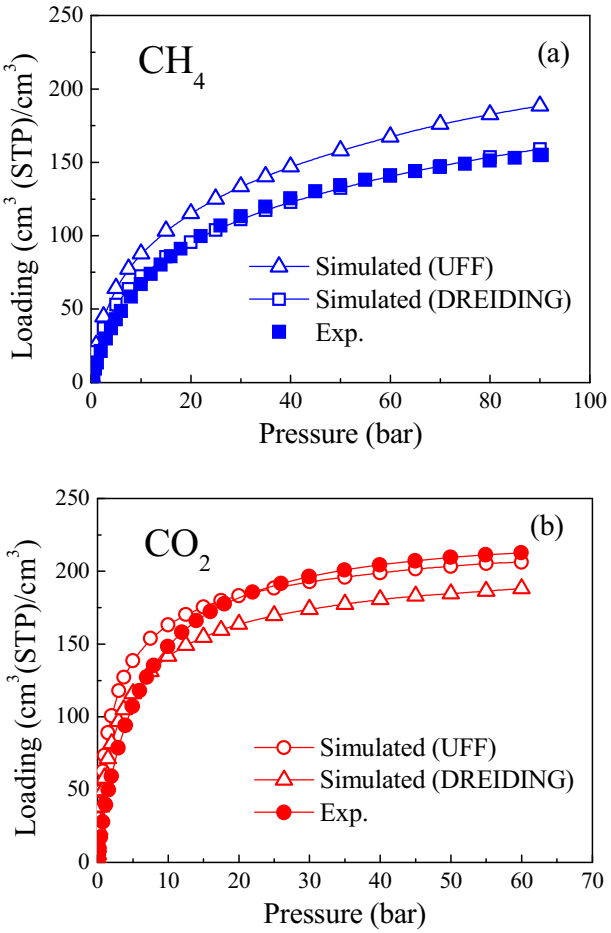


***Figure S3***: Comparison of the simulation isotherms of single gases based on different force fields with the experimental data in the dehydroxylated uiO-66(Zr) at 303 K: (a) $CH_4$, (b) $CO_2$.

## 5. Grand canonical Monte Carlo simulations

To obtain the thermodynamics correction factor used for calculating the transport diffusivity of $CO_2$ at 230 K, Grand Canonical Monte Carlo (GCMC) simulations were performed to calculate the adsorption isotherm of $CO_2$ in the dehydroxylated UiO-66(Zr) at the same temperature, using our newly developed simulation code CADSS (Complex Adsorption and Diffusion Simulation Suite). During the simulations, adsorbate molecules involved three types of trials: attempts (i) to displace a molecule (translation or rotation), (ii) to create a new molecule, (iii) to delete an existing molecule. Details on the method can be

found elsewhere.[13] The framework of the dehydroxylated UiO-66(Zr) was treated as flexible (details of the forcefield parameters in the following section). The simulation box consisted of 18 (3×3×2) unit cells for the porous material. A cutoff radius of 14.0 Å was applied to the Lennard-Jones (LJ) interactions, while the long-range electrostatic interactions were handled by the Ewald summation technique. Periodic boundary conditions were applied in all three dimensions. Peng-Robinson equation of state was used to convert the pressure to the corresponding fugacity used in the GCMC simulations. For each state point, GCMC simulations consisted of $1\times10^7$ steps to ensure the equilibration, followed by $1\times10^7$ steps to sample the desired thermodynamic properties. The simulated adsorption isotherm is shown in Figure S3 as a function of the bulk pressure, which was then fitted with the following dual-site Langmuir model,

$$c = \frac{af}{b+f} + \frac{cf}{d+f} \tag{2}$$

where $c$ is the absolute adsorption amount and f is the bulk fugacity. The fitted results are also shown in Figure S4, with the corresponding parameters a=27.94909, b=0.12318, c=19.72524, d=4.63077. As can be observed, the simulated adsorption isotherm is well reproduced by this dual-site Langmuir model.

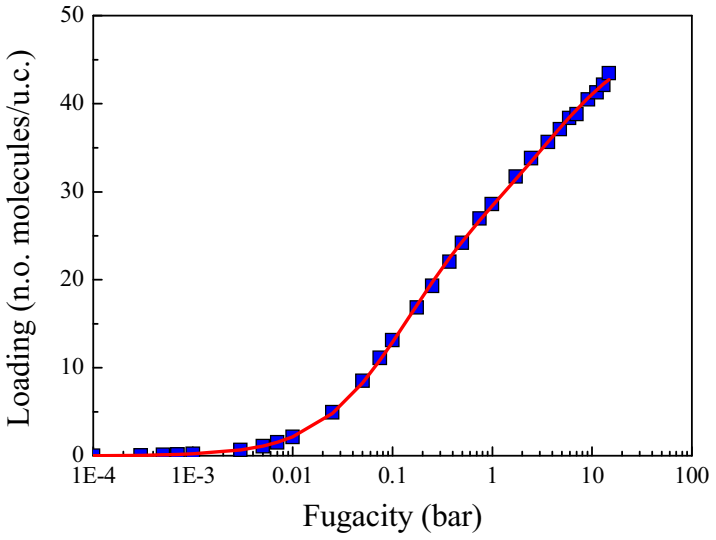

***Figure S4.*** The simulated adsorption isotherm of $CO_2$ in UiO-66 at 230 K as a function of the bulk fugacity. Simulations: blue square symbols; fitted: red line.

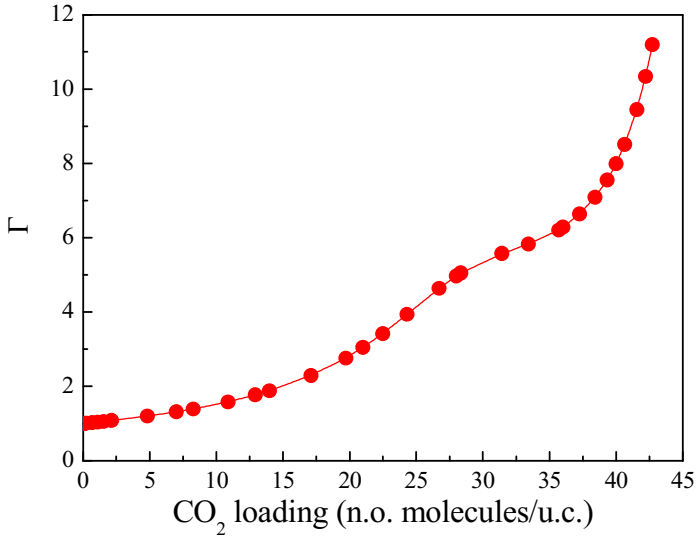


***Figure S5***. The calculated thermodynamic corrector for $CO_2$ in UiO-66(Zr) at 230 K as a function of the loading.

## 6. Molecular dynamics simulations

Based on the DL-POLY 2.20 simulation package,[14] classical molecular dynamics (MD) simulations were carried out to study the self-diffusivities of $CH_4$ and $CO_2$ gases as well as the transport diffusivity of $CO_2$ in the dehydroxylated UiO-66(Zr) at 230 K. The simulation box is also composed of 18 (3×3×2) unit cells. The calculations were performed in the canonical (NVT) ensemble for nine different loadings for $CH_4$ (4, 8, 10, 16, 20, 25, 30, 35, 40 $CH_4$ molecules per unit cell, respectively), and seven different loadings for $CO_2$ (7, 14, 21, 28, 36, 40 and 45 $CO_2$ molecules per unit cell), respectively, which cover the loadings examined by QENS measurements. Nosé-Hoover thermostat was used to maintain the constant temperature condition. It was checked that MD simulations conducted in microcanonical (NVE) ensemble lead to equivalent results. The velocity Verlet algorithm was used to integrate the Newton equations and the QUATERNION algorithm was applied for the

rotational motion of the rigid linear $CO_2$ molecules. The long-range coulombic interactions were evaluated by the Ewald summation method, while all the LJ interactions were calculated with a cutoff radius of 14.0 Å. The time step used in the MD simulations was taken as 1.0 fs, and periodic boundary conditions were applied in all three dimensions. The MD simulations were performed as follows: the molecules were randomly inserted into the pores of the MOF lattice, and then relaxed using $2\times10^5$ NVT Monte Carlo cycles. Velocities from the Maxwell-Boltzmann distribution at the required temperature were assigned to all the adsorbate molecules and the framework atoms. Further, prior to starting the production run of $2\times10^7$ MD steps (i.e., 20 ns), each MD system was equilibrated with $1\times10^6$ MD steps. The positions of each adsorbate molecule were stored every 5000 MD steps for subsequent analysis.

From these simulations, both the self-diffusivity ($D_s$) and corrected diffusivity ($D_0$) can be extracted. The self-diffusivity measures the displacement of a tagged molecule as it diffuses at equilibrium, which is related to the mean squared displacement (MSD) of tagged particles by an Einstein relation,[15]

$$D_s(c) = \frac{1}{2dN}\lim_{t\to\infty}\frac{\mathrm{d}}{\mathrm{d}t}\left\langle\sum_{i=1}^{N}\left|\mathbf{r}_i(t)-\mathbf{r}_i(0)\right|^2\right\rangle \tag{3}$$

where $\langle\cdots\rangle$ denotes an ensemble average, $\mathbf{r}_i(t)$ is the position vector of the diffusing molecule $i$ at time $t$, $N$ is the number of the adsorbate molecules in the simulation system, and $d$ corresponds to the dimension of the system examined ($d$=3 for current material).

The corrected diffusivity is related to the mean square displacement (MSD) of the center of mass of the diffusive molecules, which can also be calculated by means of an Einstein expression similar to Eq. (3), that is,

$$D_0(c) = \frac{1}{2dN}\lim_{t\to\infty}\frac{\mathrm{d}}{\mathrm{d}t}\left\langle\left|\sum_{i=1}^{N}\left[\vec{\mathbf{r}}_i(t)-\vec{\mathbf{r}}_i(0)\right]\right|^2\right\rangle \tag{4}$$

In order to improve the statistics of the calculation, the diffusivities at each loading were

averaged from five MD independent trajectories and the method with multiple time origins is also adopted as described previously.[16] For the loadings of 4 $CH_4$/u.c. as well as 7 $CO_2$/u.c., the calculations were performed at four different temperatures within the range of 230-400 K to extract the activation energies for their self-diffusivities with the linear least-squares fit to the Arrhenius equation.

Finally, the transport diffusivities were calculated from

$$D_t(c) = D_0(c)\left(\frac{\partial \ln f}{\partial \ln c}\right)_T \tag{5}$$

where the term involving the logarithmic derivative of the fugacity ($f$) related to the loading ($c$) is referred to as the thermodynamic correction factor ($\Gamma$), which can be determined from above simulated adsorption isotherm.

## 7. Flexible forcefield for the framework of the dehydroxylated UiO-66(Zr)

Recent studies in MOFs have shown that the framework flexibility has a profound influence on the diffusion of guest molecules confined in MOFs.[17,18] Thus, MD simulations were also performed to examine the effects of the framework flexibility of UiO-66(Zr) on the dynamic properties of the adsorbate species. The flexible framework of the material was modeled by the fully bonded forcefield,[17,19] where the metal-oxygen interactions were treated as covalent bonds. The flexible forcefield used for the dehyadroxylated UiO-66(Zr) was taken from our previous work,[3] where the bond stretches (Eq. 6) and bond bending (Eq. 7) were described by a simple harmonic potential function, while the bond torsion (Eq. 8) and improper torsion (Eq. 9) were expressed by the periodic cosine potential function.

$$U_{ij}^{bond} = \frac{1}{2}k_{ij}(r_{ij} - r_0)^2 \tag{6}$$

$$U_{ijk}^{bending} = \frac{1}{2}k_{ijk}(\theta_{ijk} - \theta_0)^2 \tag{7}$$

$$U_{ijk}^{Torsion} = k_{ijkl}[1 + \cos(n\phi_{ijk} - \phi_0] \quad (8)$$

$$U_{ijk}^{Improper\ Torsion} = k_{ijkl}[1 + \cos(n\phi_{ijk} - \phi_0] \quad (9)$$

where $k_{ij}$, $k_{ijk}$ and $k_{ijkl}$ are the force constants for the different interactions, $r_0$ is the equilibrium bond length separating two atoms $i$ and $j$, $\theta_0$ is the equilibrium angle involving three atoms $i$, $j$, $k$, $n$ is the periodicity, $\phi$ the dihedral angle and $\phi_0$ the factor phase.

In addition, a combination of van der Waals and electrostatic interactions (Eq. 1) were calculated only between atoms separated by more than three bonds, in which the LJ potential parameters were also taken from DREIDING forcefield,[6] as listed in Table S3. Furthermore, as done in our previous work,[16] the non-bonded interactions concerning the atoms separated by three bonds were described as 1-4 van der Waals interactions with only LJ potentials (first term in Eq. 1). All the LJ cross-interaction parameters were determined by the Lorentz-Berthelot mixing rule. The focefield has been previously validated by MD calculations in NσT ensemble to well reproduce (i) the lattice parameters (lengths, angles, and volume), (ii) the equilibrium bond distances of the various bond types of the bare dehydroxylated framework. The corresponding parameters for this flexible forcefield are listed in Table *S4*, and the labels of the different atomic types can be referred to Figure S2.

The comparison of the crystallographic features of the MD simulated structures with those previously reported from X-ray diffraction and DFT calculations is shown in Table S5 and Figure S6.

***Table S4***. Forcefield parameters for the flexible dehydroxylated UiO-66(Zr) used in this work. The definitions of the atomic types are shown in Figure S1.

| Interaction types (i-j) | **Bond stretches** |
|---|---|

| | $k_{ij}$ (kJ/(mol·Å$^2$)) | $r_0$ (Å) |
|---|---|---|
| Zr-O3 | 1077.338 | 2.098 |
| Zr-O1 | 2872.902 | 2.232 |
| C1-O1 | 4518.720 | 1.273 |
| C1-C2 | 2939.283 | 1.487 |
| C2-C3 | 4016.640 | 1.393 |
| C3-C3 | 4016.640 | 1.393 |
| C3-H1 | 3041.068 | 1.080 |
| Interaction types (i-j-k) | **Bond bendings** | |
| | $k_{ijk}$ (kJ/(mol·rad$^2$)) | $\theta_0$ (degree) |
| O3-Zr-O3 | 115.776 | 71.1 |
| O3-Zr-O3 | 115.776 | 100.4 |
| O1-Zr-O1 | 115.776 | 76.0 |
| O1-Zr-O1 | 115.776 | 81.9 |
| O1-Zr-O1 | 115.776 | 69.8 |
| O1-Zr-O1 | 115.776 | 74.4 |
| O1-Zr-O3 | 115.776 | 85.7 |
| O1-Zr-O3 | 115.776 | 124.3 |
| O1-Zr-O3 | 115.776 | 127.6 |
| O1-Zr-O3 | 115.776 | 143.5 |
| O1-Zr-O3 | 115.776 | 150.5 |
| Zr-O1-C1 | 231.637 | 135.8 |
| O1-C1-O1 | 1213.360 | 125.0 |
| O1-C1-C2 | 456.013 | 117.3 |
| C1-C2-C3 | 290.201 | 120.0 |
| C3-C2-C3 | 753.120 | 120.0 |
| C2-C3-C3 | 753.120 | 120.0 |
| C2-C3-H1 | 309.616 | 120.0 |
| C3-C3-H1 | 309.616 | 120.0 |
| Interaction types (i-j-k-l) | **Torsions** | | |
| | $k_{ijkl}$ (kJ/mol) | $n$ | $\phi_0$ (degree) |
| Zr-O1-C1-C2 | 86.837 | 2 | 180.0 |
| O1-C1-C2-C3 | 10.460 | 2 | 180.0 |
| C1-C2-C3-C3 | 12.552 | 2 | 180.0 |
| C1-C2-C3-H1 | 12.552 | 2 | 180.0 |
| C2-C3-C3-C2 | 12.552 | 2 | 180.0 |
| C2-C3-C3-H1 | 12.552 | 2 | 180.0 |
| C3-C3-C2-C3 | 12.552 | 2 | 180.0 |
| H1-C3-C2-C3 | 12.552 | 2 | 180.0 |
| H1-C3-C3-H1 | 12.552 | 2 | 180.0 |
| Interaction types (i-j-k-l) | **Improper torsion** | | |

| | $k_{ijkl}$ (kJ/·mol) | $n$ | $\phi_0$ (degree) |
|---|---|---|---|
| C2-C1-O1-O1 | 41.840 | 2 | 180.0 |
| C1-C2-C3-C3 | 41.840 | 2 | 180.0 |
| C2-C3-C3-H1 | 1.548 | 2 | 180.0 |

***Table S5***. Comparison of the MD calculated properties with those obtained by Density Functional Theory optimization.

| **Bond length (Å)** | | |
|---|---|---|
| **Bond types** | **DFT (Å)** | **MD (Å)** |
| Zr-O3 | 2.098 | 2.075 |
| Zr-O1 | 2.194 | 2.125 |
| C1-O1 | 1.273 | 1.225 |
| C1-C2 | 1.487 | 1.525 |
| C2-C3 | 1.393 | 1.425 |
| C3-C3 | 1.393 | 1.425 |
| C3-H1 | 1.080 | 1.075 |
| **Lattice parameters of the unit cell** | | |
| | **Exp.** | **DFT** | **MD** |
| α (degree) | 90 | 90 | 90 |
| β (degree) | 90 | 90 | 90 |
| γ (degree) | 120 | 120 | 120 |
| a (Å) | 14.3942 | 14.8598 | 14.7089 |
| b (Å) | 14.3942 | 14.8598 | 14.7090 |
| c (Å) | 36.1937 | 34.8904 | 35.4601 |
| Volume ($A^3$) | 6494 | 6672 | 6644 |

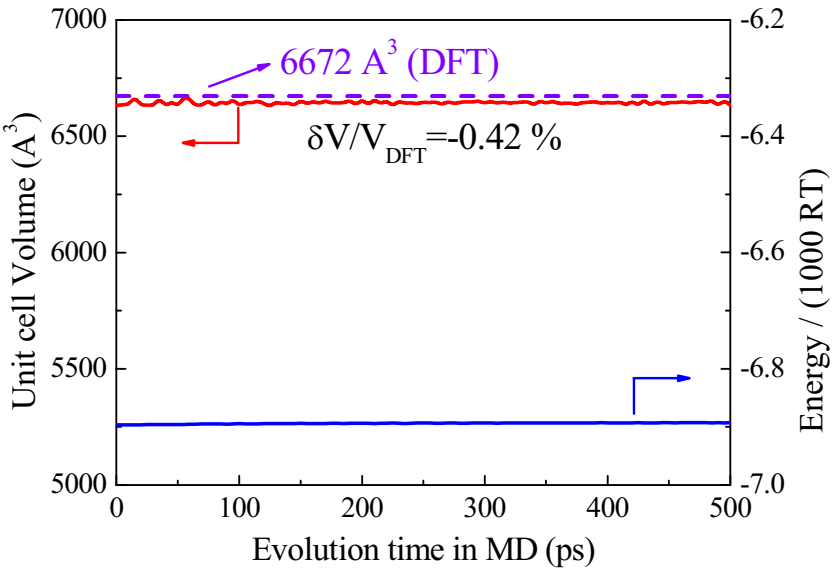


***Figure S6***. Evolution of the volume and energy with the MD times for the crystal unit cell of the dehydroxylated UiO-66(Zr) at 303 K.

## 8. Calculations of the residence times

Based on the trajectories recorded during the MD runs for both gases studied here, the average residence time inside the tetrahedral cages of the UiO-66(Zr) material was calculated for the molecules of each species as a function of the loading, respectively. In each calculation, the starting coordinates of all the molecules fore each gas stored in one MD trajectory were employed to determine whether they locate inside or outside the tetrahedral cages using the center positions and diameters of all these types of cages. The subsequent coordinates of all the molecules were used to follow whether they are entering or leaving these cages. If some molecules already inside the tetrahedral cages were found to move out of these cages, the time intervals between their entrances and current moment were then calculated.

## 9. Structural characteristics for various materials

The pore volumes of the adsorbents presented in Table S6 were obtained according to the thermodynamic method of Myers and Monson.[20] For UiO-66(Zr) considered in this work, DREIDING forcefield was used to describe the Lennard-Jones interactions of the framework atoms with Helium gas, in which the Lennard-Jones parameters for Helium ($\varepsilon/k_B$ = 10.9 K, $\sigma$ = 2.640 Å) were taken from the work of Talu and Myers.[21]

***Table S6***. Structural details of the various adsorbents related to this work

| Materials | Space group [a] | Lattice sizes [a] | Pore shape[a] | Pore size (Å) [a] | Pore volume ($cm^3.g^{-1}$) [b] |
|---|---|---|---|---|---|
| NaX (Si/Al=1.23) | FD-3 | a= 25.0280 Å, b=25.0280 Å, c= 25.0280 Å | cage/widow | 12.5/7.4 | 0.280 |
| NaY (Si/Al=2.55). | FD-3 | a= 25.0280 Å, b=25.0280 Å, c= 25.0280 Å | cage/widow | 12.5/7.4 | 0.303 |
| DDR | R-3M | a= 13.8600 Å, b=13.8600 Å, c= 40.8900 Å | cage/widow | 8.75/3.6×4.4 | 0.139 |
| CHA | R-3M | a= 13.8026 Å, b=13.8026 Å, c= 15.0753 Å | cage/widow | 8.5/3.8×4.2 | 0.264 |
| LTA | FM-3C | a= 24.6100 Å, b=24.6100 Å, c= 24.6100 Å | cage/widow | 10.0/4.1×4.5 | 0.310 |
| ZIF-68 | P63/MMC | a= 26.6407 Å, b=26.6407 Å, c= 18.4882 Å | cage/widow (GME) | 10.3/7.5 | 0.439 |
| ZIF-70 (Im:nIM=2:2) | P63/MMC | a= 27.0111 Å, b=27.0111 Å, c= 18.0208 Å | cage/widow (GME) | 15.9/13.1 | 0.729 [c] |
| MIL-47(V) | PNMA | a=6.8179 Å, b=16.1430 Å, c=13.9390 Å | channel | 8.5 | 0.606 |
| MIL-53(Cr) (LP form) | IMCM | a=16.7330 Å, b=13.0380 Å, c=6.8120 Å | channel | 8.5 | 0.518 |
| UiO-66(Zr) | R-3m | a=14.8598 Å, b=14.8598 Å, c=34.8904 Å | cage/window | 8.0-11.0/6.0 | 0.426 [d] |

[a] Obtained from XRD crystal data[22-28]

[b] Obtained from Krishna and van Baten[29]

[c] Obtained from Rankin et al.[30]

[d] Obtained in this work.

## 10. Potential barriers in UiO-66(Zr)

Figure S7 shows the potential energy surfaces experienced by $CH_4$ and $CO_2$ within the porosity of UiO-66(Zr). They were calculated by displacing a single molecule of each adsorbate along the direction linking the center of one tetrahedral cage to the center of another one, through the center of one octahedral cage. The corresponding force fields used for these calculations were the same as those mentioned above. Regarding $CO_2$, the potential energy is drawn from orientationally averaged values.

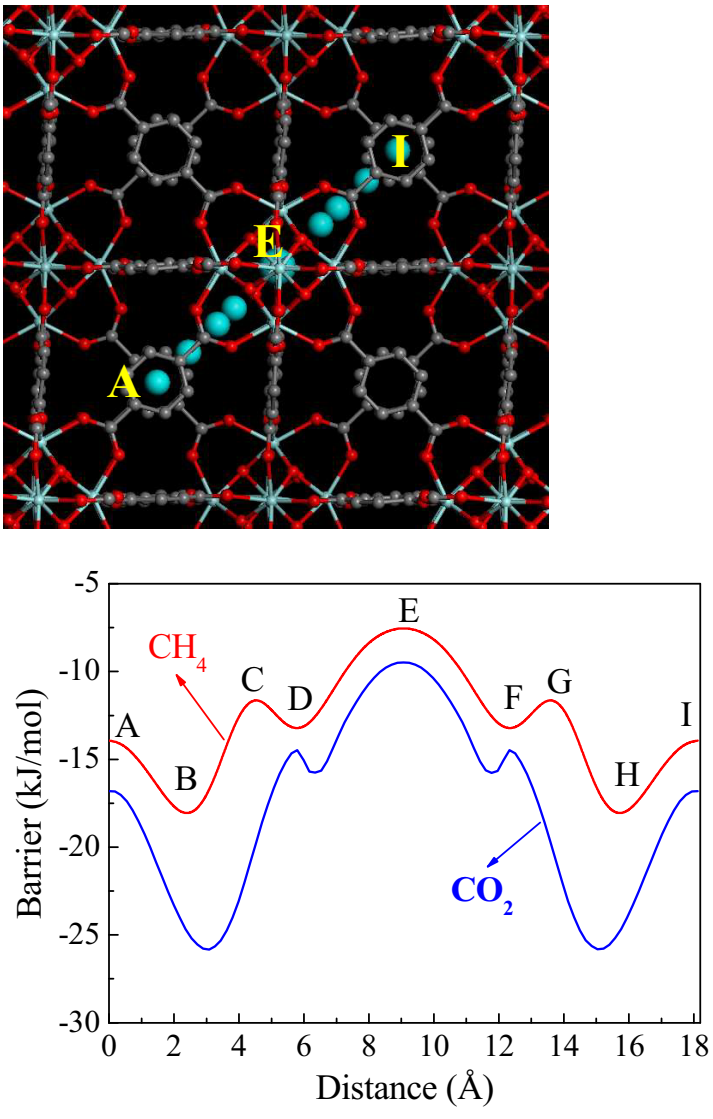


***Figure S7***. Potential energy distributions for one $CH_4$ and $CO_2$ molecule along the direction from the center of one tetrahedral cage to the center of another one, through the center of one octahedral cage.

## References:


[1] J. H. Cavka, S. Jakobsen, U. Olsbye, N. Guillou, C. Lamberti, S. Bordiga, K. P. Lillerud, *J. Am. Chem. Soc.* **2008**, *130*, 13850.

[2] H. Jobic, D. N. Theodorou, *Microporous Mesoporous Mater.* **2007**, *102*, 21.

[3] Yang et al., Submitted.

[4] M. G. Martin, J. I. Siepmann, *J. Phys. Chem. B* **1998**, *102*, 2569.

[5] J. G. Harris, K. Hung, *J. Phys. Chem.* **1995**, *99*, 12021.

[6] S. L. Mayo, B. D. Olafson, W. A. Goddard III, *J. Phys. Chem.* **1990**, *94*, 8897.

[7] A. K. Rappé, C. J. Casewit, K. S. Colwell, W. A. Goddard, W. M. Skiff, *J. Am. Chem. Soc.* **1992**, *114*, 10024.

[8] Duren, T.; Snurr, R. Q. *J. Phys. Chem. B* **2004**, *108*, 15703.

[9] Finsy, V.; Calero, S.; García-Pérez, E.; Merkling, P. J.; Vedts, G.; De Vos, D. E.; Baron, G. V. ; Denayer, L. F. M. *Phys. Chem. Chem. Phys.* **2009**, *11*, 3515.

[10] Morris, W. ; Leung, B.; Furukawa, H.; Yaghi, O. K.; He, N.; Hayashi, H.; Houndonougbo, Y.; Asta, M.; Laird, B. B.; Yaghi, O. M. *J. Am. Chem. Soc.* **2010**, *132*, 11006.

[11] Sirjoosingh, A.; Alavi, S.; Woo, T. K. *J. Phys. Chem. C* **2010**, *114*, 2171.

[12] Babarao, R.; Jiang, J. W. *Langmuir* **2008**, *24*, 6270.

[13] Q. Yang, C. Zhong, *J. Phys. Chem. B* **2006**, *110*, 17776.

[14] W. Smith, T. R. Forester, *J. Mol. Graph.* **1996**, *14*, 136.

[15] A. I. Skoulidas, D. S. Sholl, *J. Phys. Chem. B*, **2002,** *106,* 5058.

[16] F. Salles, H. Jobic, A. Ghoufi, P. L. Llewellyn, C. Serre, S. Bourrelly, G. Férey, G. Maurin, *Angew. Chem. Int. Ed.* **2009**, *121*, 8485.

[17] K. Seehamart, T. Nanok, R. Krishna, J. M. van Baten, T. Remsungnen, S. Fritzsche, *Microporous Mesoporous Mater.* **2009**, *125*, 97.

[18] J. A.Greathouse, M. D. Allendorf, *J. Phys. Chem. C* **2008**, *112*, 5795.

[19] M. Tafipolsky, S. Amirjalayer, R. Schmid, *J. Comput. Chem.* **2007**, *28*, 1169.

[20] A. L. Myers, P. A. Monson, *Langmuir* **2002**, *18*, 10261.

[21] O. Talu, A. L. Myers, *AIChE J.* **2001**, *47*, 1160.

[22] D. H. Olson, *Zeolites* **1995**, *15*, 439.

[23] H. Z. Gies, *Kristallogr*. **1986**, *175*, 93.

[24] M. Calligaris, G. Nardin, L. Randaccio, P. C. Chiaramonti, Acta Crystallogr. **1982**, *B38*, 602.

[25] T. B. Reed, D. W. Breck, *J. Am. Chem. Soc.* **1956**, *78,* 5972.

[26] R. Banerjee, A. Phan, B. Wang, C. Knobler, H. Furukawa, M. O'Keeffe, O. M. Yaghi, *Science* **2008**, *319*, 939.

[27] K. Barthelet, J. Marrot, D. Riou, G. Férey, *Angew. Chem., Int. Ed.* **2002**, *41*, 281.

[28] C. Serre, F. Millange, C. Thouvenot, M. Nogués, G. Marsolier, D. Louër, G. Férey. *J. Am. Chem. Soc.* **2002**, *124*, 13519.

[29] R. Krishna, J. M. van Baten, *J. Membr. Sci.* **2010**, *360*, 323.

R. B. Rankin, J. Liu, A. D. Kulkarni, J. K. Johnson, *J. Phys. Chem. C* **2009**, *113*, 16906-16914.